HORIZON 2020

HORIZON 2020 RESEARCH AND INNOVATION FRAMEWORK PROGRAMME OF THE EUROPEAN ATOMIC ENERGY COMMUNITY

Nuclear Fission and Radiation Protection 2018 (NFRP-2018-4)

Project acronym:	**SANDA**
Project full title:	**Solving Challenges in Nuclear Data for the Safety of European Nuclear facilities**
Grant Agreement no.:	**H2020 Grant Agreement number: 847552**

Work package:	***WP1***
Identification N°:	***D 1.8***
Type of document:	***deliverable***
Title of milestone: Report on the development and performances of the new detectors for non-energy applications	
Dissemination Level:	***PU***
Reference:	
Status:	***Achieved***
Actual Delivery date:	28 February 2022
Comments:	

	Name	Partner	Date	Signature
Prepared by:	R. Nolte	22	28-02-2022	R. Nolte
WP leader:	M. Kerveno	5	11-03-2022	<If at all possible use electronic signature>
IP Coordinator:	E. González	1	31-03-2022	Signed by E. Gonzalez at 31/03/2022 with certificate from AC Sector Público

Report on the Development and Performances of New Detectors for Non-Energy Applications

M. Dietz[1], R. Beyer[2], A.R. Junghans[2], R. Nolte[1], E. Pirovano[1], P. Vaz[3]

[1)] Physikalisch-Technische Bundesanstalt (PTB), Bundesallee 100, 38116 Braunschweig, Germany
[2)] Helmholtz-Zentrum Dresden-Rossendorf (HZDR), Bautzner Landstraße 400, 01328 Dresden, Germany
[3)] Centro de Ciências e Technologias Nucleares (C2TN), CTN - Estrada Nacional 10; 2965-066 Bobadela LRS, Portugal

Abstract

This report describes the tests carried out on silicon detectors and analog pulse-processing modules to be used at the spallation neutron source n_TOF for the measurement of double-differential cross sections for the emission of light ions in neutron-induced reactions. The tests were carried out using alpha particles from radioactive sources and proton and alpha beams from the PTB accelerators. The results are extrapolated to the energy range to be covered in the planned experiment. The performance of the detectors with respect to the γ-flash was investigated using Monte Carlo simulations. The use of gating circuits to suppress the effect of the γ-flash was studied experimentally.

1. Introduction

In particle radiation therapy for cancer, secondary neutrons with energies up to about 200 MeV (proton beams) [1] or 400 MeV (carbon ion beams) [2] are produced by beam interaction in the treatment head and in the target volume. The risk of secondary tumors induced by these neutrons has received increased interest recently [3, 4], especially for young patients. The risk assessment requires calculating the absorbed dose outside the target volume from the fluence of secondary neutrons. The required kerma factors are calculated from double-differential cross sections (DDX) for the emission of light charged particles. The experimental DDX data for tissue constituents are still rather scarce for neutron energies above 20 MeV. Data were only measured for discrete neutron energies. Close to and above 100 MeV there are only very few DDX data sets available for carbon [5-7] and oxygen [8,9]. On the other hand, the calculation of DDX data using statistical, quantum mechanical or intranuclear cascade (INC) models is difficult for low-mass nuclei and composite ejectiles [10].

Due to the large neutron energy range and the relatively small DDX values (usually less than 1 mb/(sr MeV) for $Z = 1$ ejectiles even at forward angles), evaluated data bases cannot be constructed from experimental data alone. Instead, nuclear model calculations [11] must be used. Therefore, benchmarking and improvement of codes is important in the energy region between 100 MeV and 200 MeV where the statistical model becomes invalid and the INC model just starts to become applicable. This requires experimental data at selected forward and backward angles which test the description of the intranuclear cascade and de-excitation phases of the interaction. Data for the neutron-induced emission of helium ions would be of particular importance, as complex ejectiles are not generically described in the INC model but require the ad hoc addition of a coalescence model [10].

The recent experiments for the measurement of the cross section ratio ^{235}U(n,f)/^{1}H(n,n)p at n_TOF EAR1 [12] demonstrated that the neutron-induced emission of light charged particles can be measured up to neutron energies of at least 200 MeV. The techniques developed so far will be extended to the measurement of DDX data for the neutron-induced emission of light charged particles from carbon. In contrast to the quasi-monoenergetic sources used for the earlier work, a continuous coverage of the relevant neutron energy range could be achieved at the n_TOF facility.

The experiment will focus on the energy range between 100 MeV and 200 MeV which is largely unexplored. The time during the long shutdown of the CERN PS and the commissioning of the new n_TOF spallation target was used to develop the necessary experimental equipment, i.e. a scattering chamber and detector telescopes suitable for the measurement of hydrogen and helium ions.

The most important challenge for measuring DDX at a spallation neutron source is the intense γ-flash. At n_TOF EAR1 (182 m flight path), neutron energies of 200 MeV and 100 MeV correspond to time separations of about 470 ns and 810 ns from the γ-flash. Detectors must be able to cope with intense signals induced by photons and relativistic particles from the γ-flash and from the related electromagnetic interference. Further challenges are the expected mean event rate which is determined by the moderate 'brilliance' of the spallation neutron source compared with typical quasi-monoenergetic neutron sources, the need to use thin samples to achieve low cut-off energies for the detected ejectiles and the small DDX values at larger emission angles. The goal of the project is to achieve statistical uncertainties comparable to those of the two earlier experiments at quasi monoenergetic sources [6, 7].

2. Conceptual design

The feasibility of the proposed measurement is studied for a prototype set up shown in Fig. 1. It consists of three detector telescopes positioned at emission angles of 20°, 60° and 120°. The statistical uncertainty is estimated using DDX data and the neutron fluence rate distribution at EAR1 of the n_TOF facility [13]. The solid angle is defined by the second ΔE detector. The distance of this detector to the carbon sample is 200 mm for the telescope at 20° and 150 mm for the other telescopes. An active area of 400 mm² is assumed for this detector which corresponds to the size of commercially available quadratic silicon diodes.

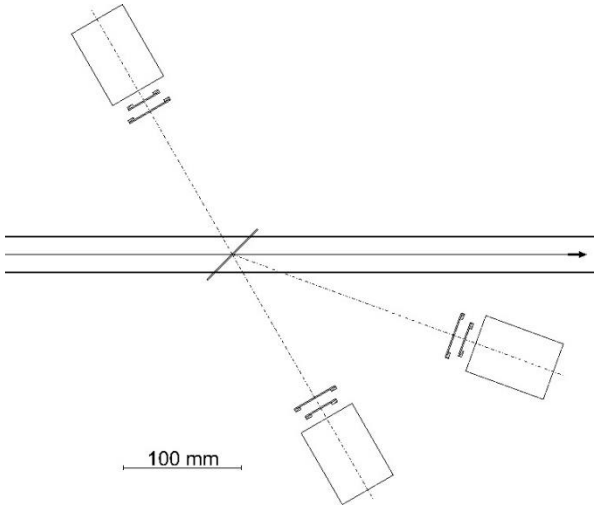

Figure 1: Conceptual set up for the measurement of DDX data at the n_TOF spallation neutron source used to study the feasibility of the experiment. The detector telescopes consist of two thin silicon diodes (50 µm and 1000 µm in thickness) and a stop detector mounted in a compact vacuum chamber (not shown on this schematic). The second silicon diode is positioned at 200 mm (20°) and 150 mm (60°, 120°) from the carbon sample. Most of the helium ions will be stopped in the second silicon diode while 200 MeV protons can be stopped in the third detector. The active area of the second silicon diode is 20 × 20 mm². This detector determines the solid angle of the telescopes. The thickness of the carbon sample is 1 mm. This conceptual set up will be optimized and, if possible, extended based on the experience gained during the test experiment.

The identification of the emitted particle species is performed by the ΔE-E method. Fig. 2 shows the expected locations of hydrogen and helium ions in the ΔE_1-ΔE_2 and ΔE_2-E matrices for a telescope consisting of 50 µm and 1000 µm thick silicon diodes and a 75 mm thick $CeBr_3$ detector.

For neutron energies below 150 MeV, the ICRU DDX data [11] were used for estimating the number of detected events. They are based on evaluation of experimental data using calculations with the GNASH code [14]. For neutron energies above 150 MeV, DDX data were calculated using MCNPX 2.7 with the INCL intranuclear cascade model. It is assumed that about $3 \cdot 10^{18}$ protons are available for neutron production which corresponds to about 30 days of n_TOF operation. This corresponds to the beam time made available for earlier experiments [12].

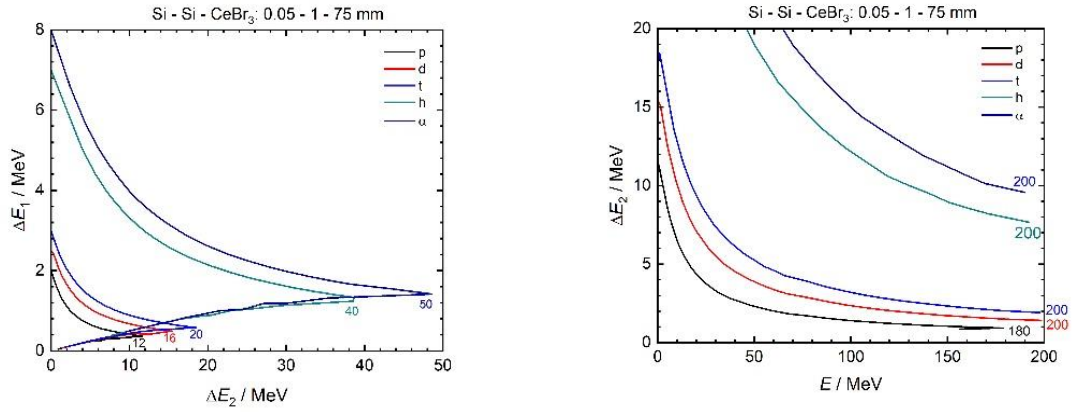

Figure 2: Identification of hydrogen (p, d, t) and helium ions (h, α) in a telescope consisting of two 50 µm and 1000 µm thick silicon diodes and a 75 mm thick $CeBr_3$ detector. The colored numbers indicate the initial energy of the respective particle.

As an example, Fig. 3 shows the ICRU DDX data [11] for the emission of protons and alpha particles for a neutron energy bin of (100 ± 5) MeV together with error bars representing the statistical uncertainty per ejectile energy bin. The expected relative statistical uncertainty is compared to that reported in EXFOR for the experiment carried out at the TSL neutron beam facility in Uppsala (Sweden) using quasi-monoenergetic 98.5 MeV neutrons. For this comparison, the uncertainties of the TSL data were re-binned to the bin structure of the ICRU DDX data. Similar calculations were carried out for neutron energies of 50 MeV, 150 MeV and 175 MeV. At the latter neutron energy, a comparison with another data set from TSL was possible [7]. Figures for the emission of deuterons are similar to those shown for the emission of protons.

The following conclusions can be drawn from these calculations:

- With the proposed prototype experiment, statistical uncertainties comparable to existing data can be achieved at forward angles for the emission of hydrogen ions.
- At backward angles and for helium ions, a better coverage of the solid angle by several telescopes positioned at the same angle or more beam time than that corresponding to $3 \cdot 10^{18}$ protons incident of the spallation target would be required.
- The sample thickness of 1 mm effects higher cutoff energies than those achieved at TSL. For helium ions, large corrections will be required for the distortions of the distribution at low ejectile energies where part of the produced particles cannot escape the sample. The corrections will introduce a significant sensitivity to the uncertainty of stopping power data and could only be avoided by using a second thinner sample and dedicated telescopes for helium ions. This, however, would increase the cost and complexity of the experimental hardware.

Despite the challenges mentioned above, the suggested prototype experiment will explore the potential of the n_TOF neutron source for a new kind of measurement in an energy range where other neutron sources are not available in Europe. The prototype experiment should aim at producing competitive data for a few selected angles to provide a reliable basis for a later decision on a more elaborate experiment.

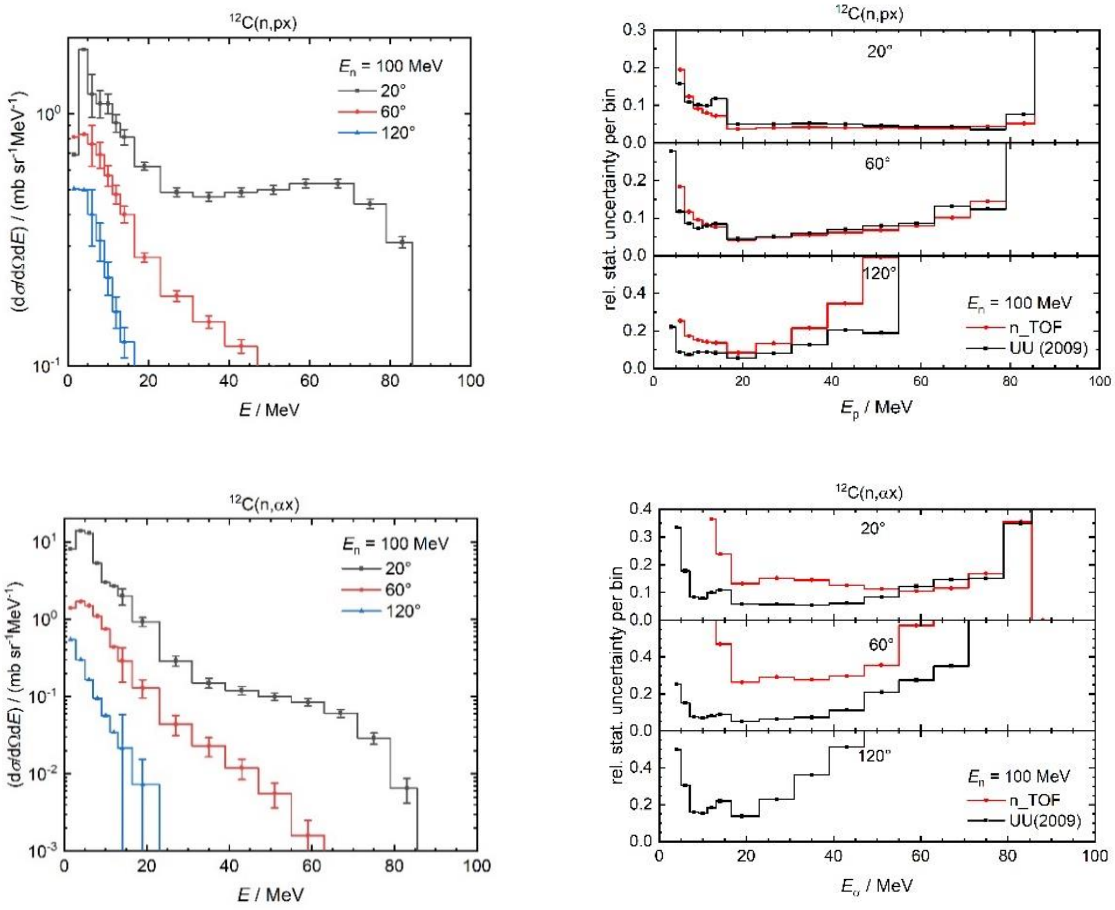

Figure 3: The left side shows DDX data for the emission of protons and ^{4}He ions from ^{12}C and expected statistical uncertainty for 100 MeV neutrons. The cross-section data are taken from Ref. [11]. The error bars indicate the statistical uncertainty per energy bin expected for the prototype experimental setup. Bins with missing error bars indicate particle energies below the cutoff imposed by finite detector thicknesses. The right side presents a comparison with the uncertainty achieved at the TSL facility [6,7], as reported in EXFOR. To facilitate a comparison, the uncertainties of the TSL DDX data were re-binned to the bin structure of the ICRU DDX data assuming statistical uncertainty contributions only. The calculations were made for a 1 mm graphite sample, assuming $3 \cdot 10^{18}$ protons incident on the n_TOF spallation target.

Compared with the earlier ^{235}U(n,f)/^{1}H(n,n)p experiment [12], the present experiment is more demanding in several aspects:

- The energy range of the ejectiles is much larger than those of the recoil protons and low cut off energies must be achieved.
- Helium ions must be detected together with hydrogen ions of much larger energy. Ion species must be separated completely.
- Per ejectile energy interval, the differential emission cross sections are considerably smaller than the n-p scattering cross section. At the same time, the sample thickness is limited by the request for low cutoff energies of alpha particles.

Therefore, as the first step, a test beam time is required to achieve the following objectives:

- Development of more compact detector configurations than in the previous experiment [12] to increase the geometrical acceptance while keeping the unwanted cross talk between detectors within reasonable limits.
- Test of the use of silicon diodes of different thickness to replace the ΔE detectors made from fast plastic scintillators used in the previous experiment. This will improve the energy resolution and the particle identification capability.
- Test of gated charge-sensitive preamplifiers to avoid saturation by signals induced by the γ-flash. This technique was already developed for an earlier experiment using Frisch-grid ionization chambers [15] and must be adapted to silicon detectors.
- Evaluation of the use of $CeBr_3$ detectors to stop energetic protons and deuterons at energies above 150 MeV.
- Optimization and, if possible, extension of the conceptual set up shown in Fig. 1, based on the experience gained during the test experiment.

In 2020, the 'Isolde and n_TOF Experiments Committee' (INTC) granted $1{\cdot}10^{18}$ protons for test experiments. Based on previous experience with the $^{235}U(n,f)/^{1}H(n,n)p$ experiment [12] at n_TOF, the beam time for detector tests will be split in two batches. This schedule will allow to react on lessons learnt from the test experiment and improve detectors before designing the final experiment. This report presents the state of the hardware development for the test experiment before the first run at n_TOF which is scheduled for May 2022.

3. Status of hardware development

3.1. Scattering chamber

The sample and the ΔE detectors (silicon diodes) must be placed in a vacuum chamber to reduce the energy loss between production of the ions in the sample and detection in the telescope. Due to their large physical size, the E detectors (plastic scintillator and $CeBr_3$ scintillator) required to stop protons and deuterons with energies approaching 200 MeV will be placed outside the scattering chamber behind thin windows. This will also allow easy readout of the scintillation detectors using photomultiplier tubes.

The scattering chamber must be adapted to the technical constraints at n_TOF EAR1, where physical space is limited and equipment for handling heavy devices is not available. For the first test experiment, an existing 400 mm diameter light-weight aluminum scattering chamber will be used. The chamber was originally designed for use with ion beams and small detectors. For the test experiment with neutron beams, the height of the chamber was extended from 70 mm to 150 mm to accommodate larger detectors and reduce potential problems with stray particles. The chamber has eight 47 mm diameter flanges with an angular separation of 45° originally used to hold signal feedthroughs. Four of these flanges were equipped with 50 µm Kapton vacuum windows for the ingoing and outgoing neutron beam and for two full ΔE_1-ΔE_2-E telescope arms at 45°, 90° or 135°. As shown in figure 4, the chamber was also employed for detector tests using scattered protons and alpha beams from the PTB accelerators. The chamber is equipped with a SCROLLVAC pump which reaches a residual gas pressure of about 1 Pa – 10 Pa in the chamber which is lower than required for the purpose.

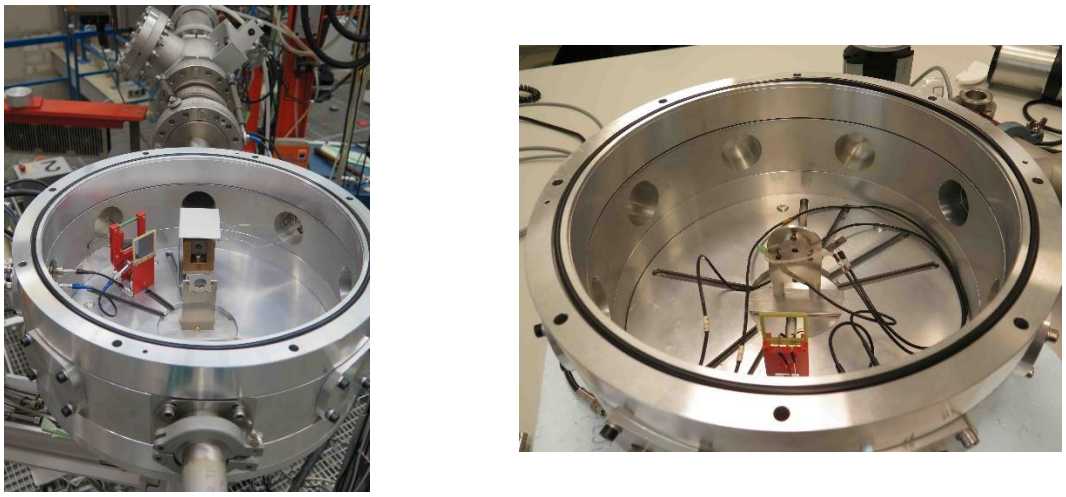

Figure 4: The left panel shows the upgraded scattering chamber mounted at beam line 2 of the PTB ion accelerator facility. The silicon detectors are tested using protons and alpha particles scattered from a 0.5 µm gold foil in the center of the chamber. The right panel shows diode tests using the ^{241}Am/^{244}Cm/^{239}Pu alpha source and LEDs producing light pulses with duration of about 10 ns – 100 ns.

3.2. Silicon detectors: Energy resolution and particle identification

The ion-implanted silicon diodes presently available for the DDX measurement were manufactured by Micron Semiconductor Ltd. and by Canberra Semiconductors N.V. Table 1 gives an overview of the available sizes and thicknesses together with a few other parameters. The quadratic diodes are mounted on small printed-circuit board frames which make it possible to use the diodes as transmission detectors.

Table 1: Parameters of the silicon diodes purchased for the first test. The thickness d_{dep}, voltage U_{dep} and capacity C_{dep} at full depletion are typical values which vary slightly between individual pieces. The resolution (FWHM) ΔE_α quoted by the manufacturers is for ^{241}Am alpha particles (E_α = 5.486 MeV). The MSX09 and MSX04 diodes were manufactured by Micron Semiconductor Ltd and the RF30*30-500EB diodes by Canberra Semiconductors N.V.
[1)] No specification by the manufacturer.

Pieces	Type	A / mm²	d_{dep} / µm	U_{dep} / V	C_{dep} / pF	ΔE_α / keV
2	MSX09	900	1000	145	110	45
2	MSX09	900	500	40	210	55
2	MSX09	900	300	23	340	[1)]
2	MSX09	900	50	3	2100	200
1	MSX04	400	60	10	850	55
4	RF30*30-500EB	900	500	70	[1)]	19

As can be seen from table 1, the RF30*30-500EB diodes offer a better resolution but are only available with thicknesses of 500 µm and 300 µm. They are also more expensive than the MSX diodes. Hence, MSX diodes will have to be used in most cases.

The different diodes were evaluated using a ^{239}Pu/^{241}Am/^{244}Cm mixed nuclide alpha source, a Canberra 2004 preamplifier and a Tennelec 242 shaping amplifier with a shaping time of 1 µs and a Silena UHS ADC. Figure 5 shows the pulse-height distributions of a RF30*30-500EB diodes and an MSX04-50 diode to demonstrate the variation in resolution among the diodes of different sizes and thicknesses. The resolution obtained for the dominant alpha lines is roughly consistent with the values quoted by the manufacturer.

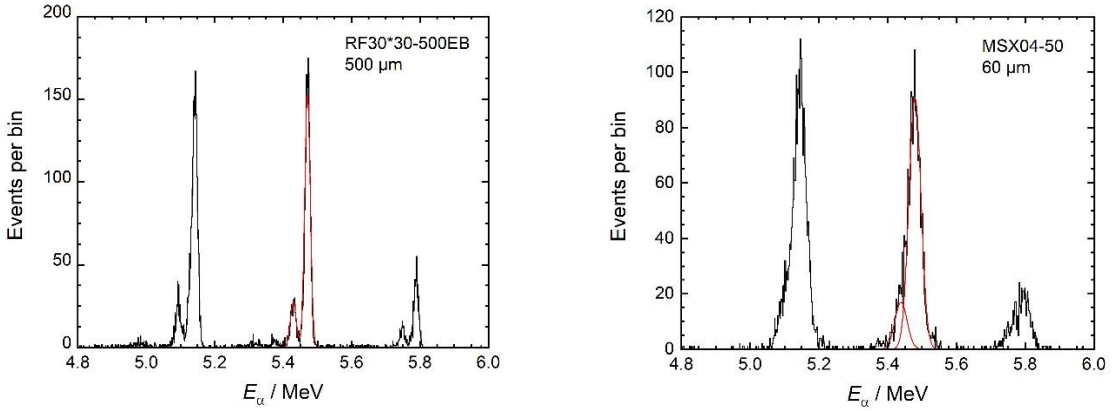

Figure 5: Pulse-height distributions for a RF20*30-500EB (500 µm) diode (left panel) and an MSX04 (60µm) diode (right panel) produced by alpha particles from a ^{239}Pu/^{241}Am/^{244}Cm source. The resolution quoted by the manufacturers for ^{241}Am alpha particles (E_α = 5.486 MeV) is 22 keV (0.40%) for the RF30*30-500EB diode and 55 keV (1.00%) for the MSX04 diode. The measurements were carried out using a Canberra 2004 preamplifier, a Tennelec 242 shaping amplifier with a shaping time of 1 µs and a Silena UHS ADC. The red lines show a decomposition of the energy distribution of alpha particles from the decay of ^{241}Am.

Table 2 gives an overview about all diodes tested so far.

Table 2: Pulse-height resolution $\Delta E_\alpha/E_\alpha$ (FWHM) for ^{239}Pu alpha particles (E_α = 5.157 MeV) measured using a Canberra 2004 preamplifier, a Tennelec 242 shaping amplifier with a shaping time of 1 µs and a Silena UHS ADC. ΔE_α denotes the full width at half maximum (FWHM).

Type	$\Delta E_\alpha/E_\alpha$
Micron MSX09 1000 µm	0.68%
Micron MSX09 500 µm	0.65%
Micron MSX04 60 µm	0.80%
Micron MSX09 50 µm	1.50%
Canberra RF30*30-500EB	0.52%

The first signal processing stage behind the detector was always a charge-sensitive preamplifier which integrates the current signal produced in the detector. Analog signal processing of the preamplifier output signal using a standard shaping amplifier with microsecond shaping times still shows the best performance. For measurements at n_TOF, however, this is not a viable option because of the high instantaneous event rates. The n_TOF data acquisition uses SP Devices Digitizers to record the full waveform over several milliseconds. For the DDX experiment, the relevant time window extends only to several microseconds after the arrival of the fastest neutrons. To avoid pile up of consecutive events in this time frame, a much faster shaping is required at the expense of adding additional noise which impairs the resolution. Therefore, several options are conceivable:

- Shaping of the output signals from standard charge-sensitive preamplifier, e.g. Canberra 2004, using separate wideband fast-filter amplifiers (FFAs) with shaping and differentiation time constants in the order of 20 ns to 40 ns to produce signals with a total width of about 130 ns. This procedure was successfully used in earlier experiments at n_TOF to handle signals from fission ionization chambers.
- Use of integrated preamplifier-shaper combinations developed for ultra-high rate spectroscopy with diamond detectors (Cividec Cx-L, CAEN A1425). The dynamic range of these modules must be adapted to the use with silicon diodes because of the smaller *w*-value of silicon compared with diamond.
- Direct recording of the waveform produced by the charge-sensitive preamplifier and offline numerical shaping of the signal.

The first two options were tested in the laboratory using alpha particles from the decay of ^{239}Pu. The third option requires data taken under the actual count-rate and noise situation encountered at EAR1 of n_TOF. Hence, this must be left to after the first test run. In an attempt to anticipate problems related to saturation effects induced by the γ-flash, the effect of an electronic gate ('switch') between the detector and the preamplifier input on the resolution was investigated.

Table 3: Resolution $\Delta E_\alpha/E_\alpha$ of the Micron and Canberra diodes for ^{239}Pu alpha particles (E_α = 5.157 MeV) using different analog signal processing stages. The signals were digitized using an ADQ14 digitizer of SP-Devices. This digitizer is also used in the n_TOF DAQ system. The 'switch' is an electronic gate between the diode and the preamplifier input. This gate module was manufactured at PTB following the HZDR design [13].
1) This combination was meant as a reference only and is not a viable option for a measurement at n_TOF because of the long shaping time of the Tennelec 242 amplifier.

	MSX09 1000 µm	**MSX09 500 µm**	**MSX04 60 µm**	**MSX09 50 µm**	**RF30*30-500EB 500 µm**
Canb. 2004 + Tennelec 242[1)]	0.6 %	0.9 %	1.3 %	2.0 %	0.6 %
Canb. 2004 + ORTEC 579	2.6 %	2.4 %	2.6 %	7.3 %	1.8%
Cividec Cx-L	1.1 %	1.3 %	2.6 %	5.8 %	1.2 %
Switch + Cividec Cx-L	1.3 %	1.5 %	3.1 %	8.8 %	1.3 %
CAEN A1425	2.1 %	2.9 %	3.0 %	4.3%	2.2%
Switch + CAEN A1425	2.4 %	3.2 %	3.8 %	5.5%	2.4%

The results shown in table 3 can be summarized as follows:

- The use of the 14 bit/1 GS waveform digitizer ADQ14 instead of a 'classical' pulse-height sensitive ADC does not lead to a relevant loss of resolution.
- As expected, the fast shaping required for n_TOF effects a deterioration of the resolution. The best option is the use of the preamplifier – shaper combination Cividec Cx-L. The combination of the of-the-shelf modules Canberra 2004 preamplifier and ORTEC 579 fast filter amplifier offers more flexibility in selecting gain and shaping time constants but is inferior with respect to the resolution achieved.
- The installation of the 'switch' in front of the preamplifier causes only a slight increase of the resolution, except for the very thin 50 µm diode with its large capacity. It should be noted here that the most recent version of the 'switch' manufactured at the HZDR workshop was specially adapted to the capacity range of the present detectors and showed no additional contribution to the resolution. A final test of this module with the present test setup is still pending.

The tests of single diodes using alpha particles from radioactive sources were complemented with tests using protons and alpha particle beams from the 2 MV Tandetron and the CV28 cyclotron of the PTB ion accelerator facility PIAF. The beam particles were scattered at angles of 135° or 112° from a 0.5 µm gold foil to reduce the event rate to about 10^2 s^{-1} - 10^3 s^{-1}. The setup is shown on the left panel of figure 4. Tests with 3 MeV and 4 MeV protons confirmed that the resolutions of the MSX09 diodes with thicknesses of 500 µm and 1000 µm were consistent with the resolution measured with ^{239}Pu alpha particles when the effect of energy loss and straggling in the gold foil was corrected for and a $1/\sqrt{E}$ scaling law was applied for extrapolation.

The resolution of a thin diode used as a transmission (ΔE) detector in a ΔE-E telescope increases due to the fluctuation of the energy loss when the range of the ions exceeds the thickness of the transmission detector. For the rear stop (E) detector, the relative contribution of other sources of noise increases because only a small amount of energy is deposited in this detector when the initial energy of the ion is just above the 'punch-through' energy of the ΔE detector. Figure 6 shows the pulse-height distributions measured for a telescope configuration consisting of an MSX09 50 µm diode (ΔE) and an MSX09 1000 µm diode (E) using 10 MeV alpha particle scattered at 135°. At this angle, the scattered alpha particles have a maximum energy of 9.33 MeV. The distributions of the deposited energy were

calculated using MCNPX, folded with a Gaussian and fitted to the experimental distributions. The thickness of the 50 µm diode had to be reduced from its nominal value of 49 µm to 46 µm to achieve a consistent match of the centroids of the measured distributions of charge-equivalent energies ΔE, E and ΔE+E. This measurement is a relevant example for the performance of the selected detectors because the range of the alpha particles is only 63 µm, i.e. only slightly larger than the thickness of the ΔE_1 detector. The experimentally observed relative widths (FWHM) of the ΔE and E distribution amount to 8.2% and 24.2%, whereas resolutions of 5.7% and 8.0% would be extrapolated from the resolution measured for ^{239}Pu alpha particles. The relative width of 5.1% observed for the ΔE+E distribution, however, is relatively close to the extrapolated resolution of 4.6%.

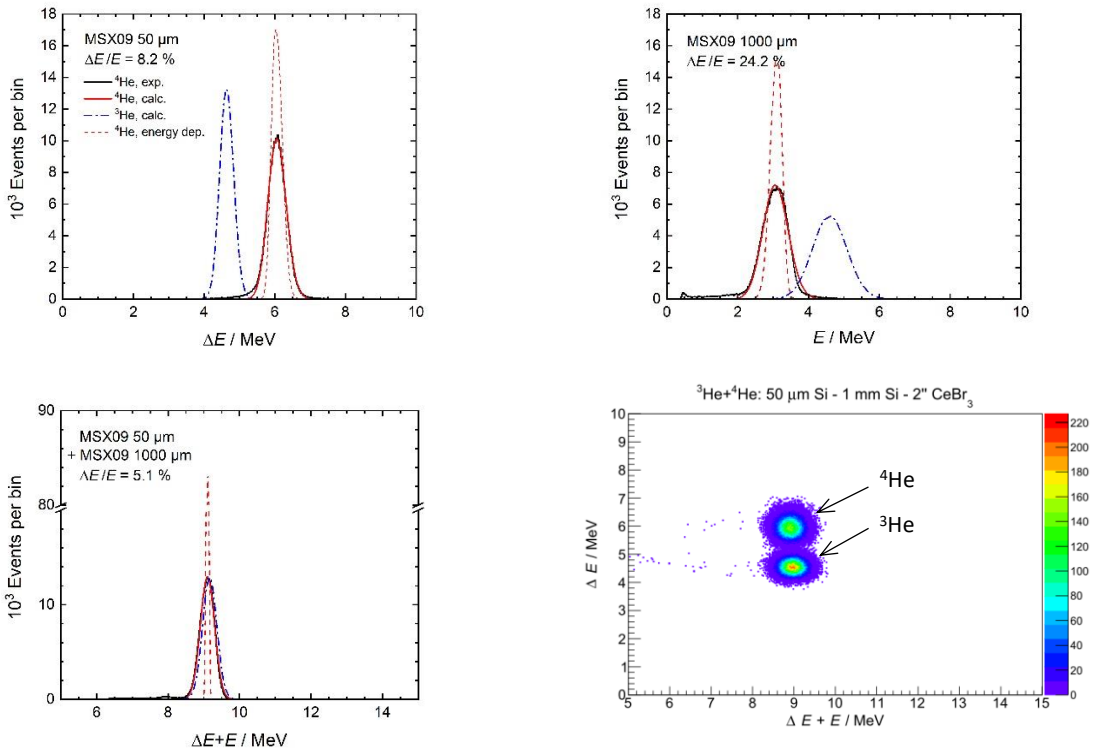

Figure 6: Distributions of charge-equivalent deposited energy measured for a telescope configuration consisting of an MSX09 50 µm diode and an MSX09 1000 µm diode using 10 MeV alpha particle scattered at 135°. At this angle, the energy of the scattered alpha particles is 9.33 MeV. The black histogram are the experimental data. The distributions of deposited energy calculated with MCNPX are shown by the dashed red line. The solid red lines are the calculated distributions after folding with a Gaussian of constant relative width $\Delta E/E$ (FWHM) to match the experimental data. The blue dashed-dotted lines show distributions of deposited energy calculated for ^{3}He particles of the same kinetic energy, assuming the same resolution as for the alpha particles. The lower right panel shows the calculated two-dimensional distributions of ^{3}He and ^{4}He events.

Unfortunately, a single data point is not sufficient to predict in detail the performance of the particle separation capability over the full energy range to be covered in the n_TOF experiment. Therefore, figure 6 just shows calculated deposited energy distributions to be expected for ^{3}He particles of the same kinetic energy as the alpha particles, assuming the same resolution $\Delta E/E$ for the two helium isotopes.

3.3. Suppression of the γ-flash in silicon detectors

The intense γ-flash at EAR1 is a special challenge for the use of charge-integrating preamplifiers. This is illustrated in figure 7 which shows waveform from an earlier test measurement with a two-stage Δ*E*-*E* telescope consisting of a 500 µm RF30*30-500EB diode and an 80 mm long cylindrical EJ204 plastic scintillator.

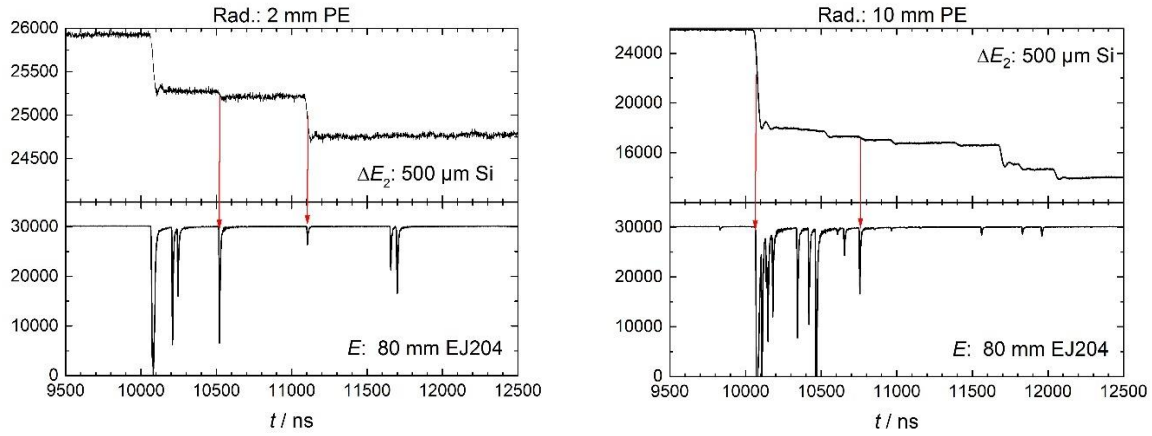

Figure 7: Waveforms acquired for telescope consisting of a 500 µm RF30*30-500EB silicon diode (upper panels) and plastic scintillator (lower panel) in an earlier experiment. The leftmost step in the diode waveform is the signal induced by the γ-flash. The intensity of the signal induced by the γ-flash depends on the number of protons in the bunch, the thickness of the sample scattering the photons into the diode and the thickness of the diode. The 10 mm polyethylene (PE) sample used for the example on the right panel is rather thick but the example on the left panel is representative for the conditions expected for the DDX experiment. The red arrows mark coincident events in the Δ*E* and *E* detector.

Depending on the number of protons per bunch impinging on the n_TOF spallation target, the thicknesses of the radiator and of the diode, a considerable amount of charge is induced by photons of the γ-flash scattered into the detector. This charge can already exhaust part of the dynamic range of the preamplifier before the first useful signal is detected. Consequently, this could lead to loss of valid events due to early saturation of the preamplifier.

To be prepared for such problems, the use of gating circuits inserted between the diode and the preamplifier input was investigated. These so-called 'switches' were developed by a collaboration of HZDR, CERN and IPNO for use with gridded ionization chambers [15]. They drain the charge induced in the detector to ground during the occurrence of the γ-flash. After the γ-flash, the preamplifier is reconnected and its full dynamic range can be used for acquiring useful signals. Gating circuits following the HZDR design were manufactured at PTB and compared with circuits adapted at HZDR to the input capacities of the diodes to be used for the present experiment. The focus was on the stability of the gating circuit, the suppression of 'switching spikes' and the deterioration of the resolution effected by the noise of the switching circuit. In a test setup, the 'switch' function of the PTB design was investigated using a pulsed LED to simulate the γ-flash by a flash of photons in the visible range. Figure 8 shows a waveform from the 500 µm Canberra diode and the gate signal which triggers the switch circuit to drain the charge pulse to ground when the gate signal is active. The oscillations close to the leading and trailing edges of the gate signal are 'switching spikes' and still under investigation. Especially the trailing spike should be reduced as much as possible to avoid distortions of valid signals from neutron-induced events close to the γ-flash.

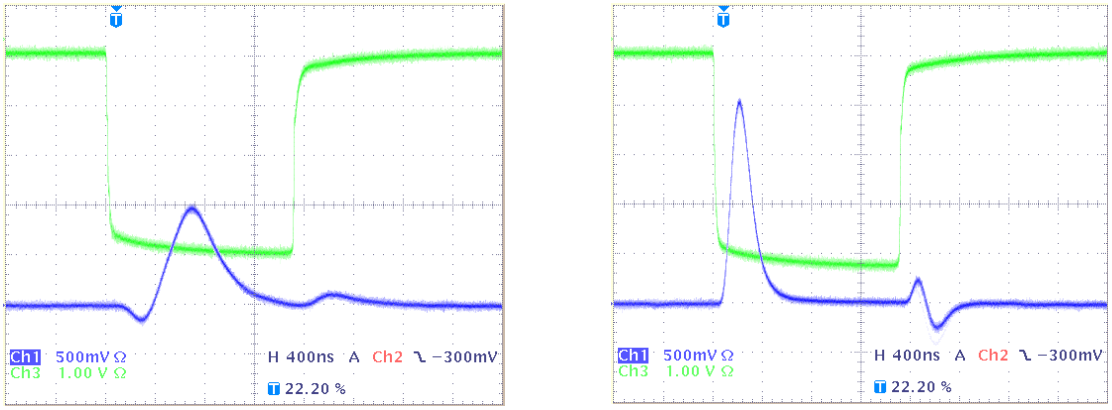

Figure 8: Waveform of a 500 µm RF30*30-500EB silicon diode read out by a Cividec Cx-L amplifier (blue). The γ-flash was simulated by irradiating the diode with light pulses from an LED. The second waveform (green) is the gate signal, which defines the interval when the diode signal is drained to ground. On the left panel, this gate signal is not connected to the 'switch' and the LED signal is visible in the preamplifier output signal. On the right panel, the gate is connected and the LED signal is suppressed. Unfortunately, the gate signal induces small fluctuations, which are enhanced by the shaping amplifier. These 'switching spikes' of a few hundred mV are still under investigation and subject of optimization through different adaptation in the switch design.

3.4. Scintillation detectors

The energy distribution of the more energetic light charged particles, especially the hydrogen ions at forward angles, must be determined from the pulse height measured in the *E* detectors. For an earlier experiment, cylindrical EJ204 plastic scintillation detectors were used to detect recoil protons up to 150 MeV. These detectors have a fast time response and the low-*Z* material reduces the sensitivity to the γ-flash but their low density makes it impossible to stop protons above 150 MeV while keeping the size of the detectors manageable. With inorganic scintillators higher maximum proton energies could be reached but the increased γ-ray sensitivity, slower time response compared with organic scintillators and especially the strong afterglow of most inorganic scintillators could be a problem. The most promising candidate in this respect is $CeBr_3$ which is fast and has a relatively low afterglow.

A first parasitic test was carried out with a small 1.5" x 1.5" crystal in 2021. The $CeBr_3$ detector was installed at EAR1 outside the beam upstream in 20 cm distance from a 2mm thick ^{80}Se sample. Figure 9 shows waveforms produced by γ-flash photons scattered from the sample. The first peak results from the γ-flash and following signals are already registered after a few hundred nanoseconds, which is very promising for measurements at high neutron energies. A small change in the baseline between 1 µs and 3 µs after the γ-flash was observed which could result from ion-feedback ('rebound') in the photomultiplier, but this can be accounted for in the pulse recognition software. This result motivated the purchase of a larger 2" x 3" $CeBr_3$ crystal which can stop 200 MeV protons and will be used at the forward angles of the DDX experiment. At the larger angles, the existing EJ204 plastic scintillation detectors will be employed.

When a charged particle is stopped in a detector, the amount of scintillation light collected by the photomultiplier depends on penetration depth of the particle in the detector, i.e. on its kinetic energy. Therefore, the spatial dependence of the light collection efficiency is required to convert the measured amount of scintillation light into the kinetic energy of the particle at the entrance into the detector.

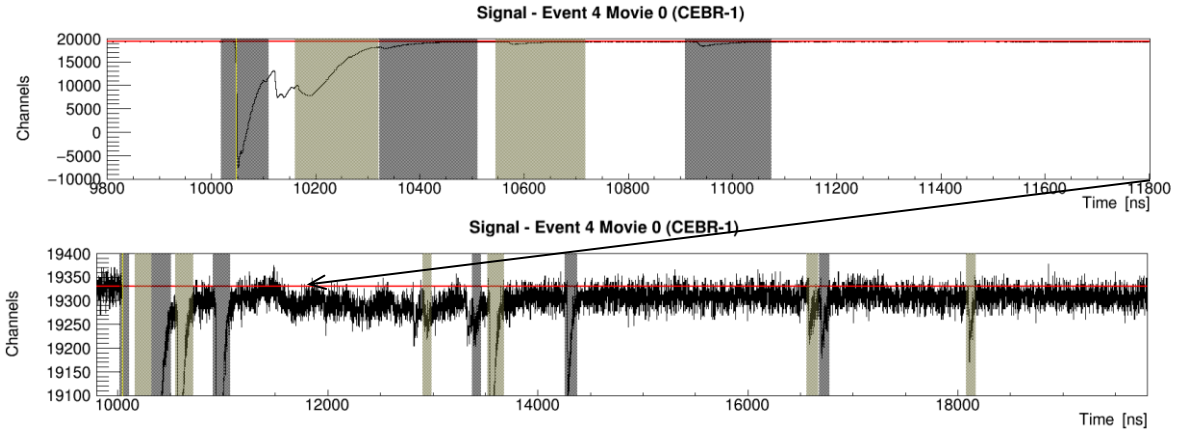

Figure 9: Waveforms acquired with a 1.5"x 1.5" $CeBr_3$ detector which was placed outside the neutron beam at a distance of about 20 cm from a 2 mm thick ^{80}Se sample. The upper panel shows the large signal induced by the γ-flash in a 2 µs time window, while the lower panel shows the same event in a wide 10 µs time window with an expanded view on small signals and the relatively quick recovery of the baseline. There is evidence that signals can already be recognized at about 400 ns after the γ-flash which corresponds to neutron energy of 240 MeV.

For one of the existing EJ204 detectors, this was investigated by scanning the detector with an actively collimated photon source. The active collimation has been realized by requesting a coincidence of the signal produced by 511 keV annihilation photons from a ^{22}Na source with the signal produced by the second 511 keV photon in a second small BaF_2 detector positioned at a larger distance. The line integrals of the light collection efficiency can be compared with model calculations using a dedicated 'ballistic' Monte Carlo model of optical photon transport. This simple model describes the optical photons as 'particles' which interact with optical interfaces according to Fresnel's law of reflection and refraction or Lambert's law of diffuse reflection combined with specular reflection and worked quite well for small and thin scintillation detectors surrounded by diffusive reflectors. The investigations were carried out in an attempt to provide a complete map of the light collection efficiency.

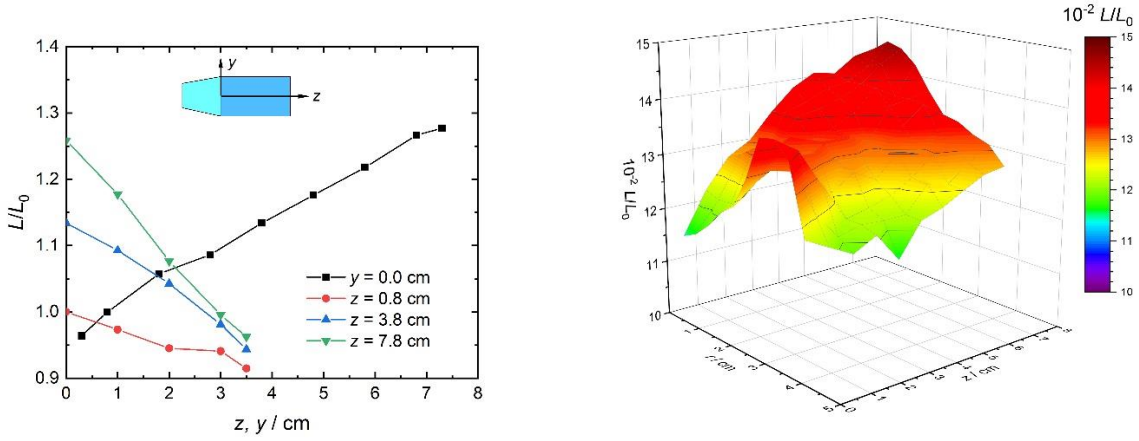

Figure 10: Relative light collection efficiency L/L_0 in an 80 mm long cylindrical EJ204 E detector equipped with a conical light guide. Here $L(\boldsymbol{x})$ denotes the number of scintillation photons collected at the photomultiplier cathode for a scintillation event a point $\boldsymbol{x}$ in the detector. The left panel shows line integrals of the relative light collection efficiency for a scan along and perpendicular to the rotational axis using an actively collimated beam of 511 keV annihilation photons. The right panel shows a map of the light collection calculated with a transport model for optical photons. The reflection properties of the surfaces were adjusted to the experimentally observed trends.

As an example of the results obtained so far, figure 10 shows measured line integrals of the relative light collection efficiency for scans along and perpendicular to the rotational axis of the detector together with a two-dimensional map calculated with the Monte Carlo model.

After adjustment of the reflection properties of the surfaces, the general trends are reproduced, e.g. the increased light collection efficiency along the axis towards the front surface of the detector or the decrease in radial direction. Other details, for example those next to the interface between the conical light guide and the scintillator, still deviate considerably. This demonstrates the need for further work in this direction, for example using the capabilities of Geant4, as an entirely experimental characterization would be very laborious.

3.5. Status of detector simulations

The expected detector performance was studied using the MCNPX Monte Carlo code. The most important questions are the expected effect of the γ-flash and the separation of the different light ion species by the ΔE-E method.

Figure 11 shows the source term for the energy distribution for the γ-flash photons. It was taken from the results of extensive simulations carried out for the second n_TOF spallation target [13]. With these input data, MCNPX was used to calculate the energy deposited per proton beam pulse for silicon detectors of different thicknesses and for a $CeBr_3$ stop detector.

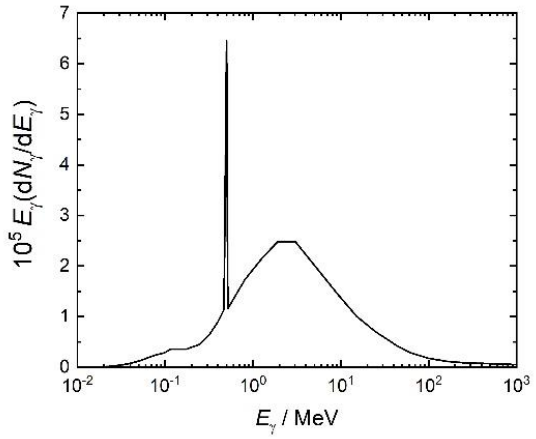

Figure 11: Energy distribution of prompt photons at EAR1 using the capture collimator configuration. The data are normalized for a beam pulse containing $7 \cdot 10^{12}$ protons and were taken from [13].

The detectors were embedded in a 2 m diameter sphere filled with air to include the effect of the interaction of photons with the air between the exit window of the n_TOF beam tube and the position of the experiment. The shielding effect of the scattering chamber on the silicon detectors was ignored. The sample hit by the γ-flash was a 1 mm thick graphite disk. To identify the influence of the air, the same simulation was also carried out with the primary photons transported in vacuum except for the sample. Table 4 summarizes the results.

The simulations indicate that about half of the signal induced by the γ-flash results from the interaction with the air between the exit window and the scattering chamber. Therefore, a vacuum tube bridging this gap would be beneficial to reduce the signal induced by the γ-flash. Without this tube, a considerable part of the dynamic range of the preamplifier connected to the thicker diodes would be 'exhausted' by the γ-flash. As expected, this problem is less severe for the thin diodes.

Table 4: The energy E_{dep} deposited per beam pulse in a telescope consisting of two 900 mm² silicon diodes and a 2"×3" $CeBr_3$ crystal was calculated using MCNPX. The distance between the first diode and the 1 mm graphite sample was 10 cm and the angle with respect to the neutron beam was 45°. The number of protons per beam pulse was $7 \cdot 10^{12}$ which is standard for beam pulses dedicated for the n_TOF facility. The charge induced in the silicon diode is $Q_{dep} = e_0 E_{dep}/w$, where w = 3.62 eV is the energy required to produce an electron-hole pair in silicon. The resulting voltage step U at the preamplifier output refers to a charge-sensitive preamplifier with a sensitivity of 1.2 mV/fC and a linear range of 2 V, as for the adapted Cividec Cx-L modules. The detectors were embedded in a 2 m diameter sphere filled with air at ambient pressure.

	Air (1 m)			Vacuum		
Detector	E_{dep} / (MeV)	Q_{dep} / fC	U / mV	E_{dep} / (MeV)	Q_{dep} / fC	U / mV
50 µm Si	1.45	64.7	77.7	0.99	43.9	52.7
1000 µm Si	16.6	744.8	893.8	8.80	391.7	470.0
76.2 mm $CeBr_3$	122.4			32.7		
76.2 mm EJ204	76.1			6.41		

As discussed above, the detailed prediction of particle identification requires more experimental data on the resolution of the transmission detectors than presently available from the beam experiments. Therefore, the distributions of deposited energy calculated using MCNPX and the LA150 library can only show trends. The resolutions of the silicon diodes were extrapolated from the data measured with ^{239}Pu alpha particles and Cividec Cx-L preamplifiers (see table 3), assuming a $1/\sqrt{E}$ dependence. For the $CeBr_3$ stop detector an energy independent resolution of 10% was assumed to account for the spatial inhomogeneity of the light collection efficiency.

The example shown in figure 12 was obtained for neutrons with energies between 90 MeV and 110 MeV. The LA150 library contains cross section data for the emission of protons, deuterons and ^{4}He ions. Compared with these ions, the cross sections for the emission of tritons and ^{3}He ions are considerably smaller. Hence, they are not included in the library and therefore not visible in the calculated distributions. The present example shows that separation of the different hydrogen and helium isotopes should be possible if the measured resolutions can be achieved under the technical conditions of an experiment at n_TOF EAR1. If the resolutions would increase by a factor of two, however, complete separation of the different ion species would be impossible, at least at lower energies.

4. Plans for the first and second test beam time

The test beam time granted by the INTC will be split in two parts that are scheduled for May and November 2022. The first run will focus on studying the immunity of the setup to electromagnetic interference and on the possible saturation effects caused by the γ-flash. Telescopes set up from diodes of different thicknesses will be tested to avoid 'gaps' in the data due to cutting out the difficult 'punch-through' regions where the hydrogen ions are no longer stopped in the second ΔE detector. As demonstrated above, the final test for the performance of particle separation can only be conducted with a broad neutron beam and under the actual technical conditions at n_TOF. In case of a successful first test run, an application for beam time for a production run will be prepared for the next meeting of the INTC. In the second run will be used to take data with a close-to-final setup for developing analysis procedure for the production run.

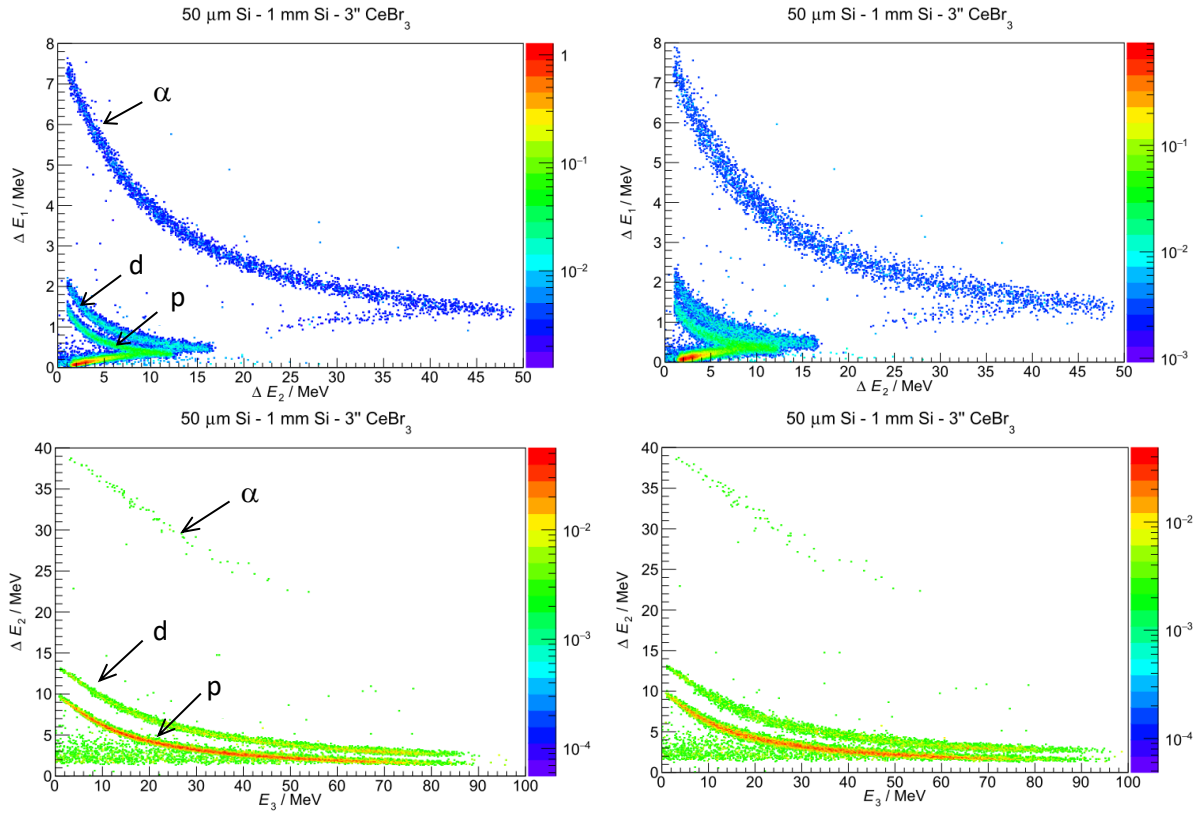

Figure 12: Simulation of the identification of the different light ion species in a prototype telescope consisting of two 900 mm^2 silicon diodes, 50 µm and 1000 µm in thickness and a cylindrical $CeBr_3$ detector, 76.2 mm in length and 50.8 mm in diameter. The calculations were carried out using MCNPX and the library LA150. Neutrons with energies between 90 MeV and 110 MeV were incident on a 0.5 mm graphite sample. The resolution of the 50 µm and 1000 µm silicon diodes used as transmission detector were obtained from measurements with ^{239}Pu alpha particles (left panels). The right panels show distributions calculated for resolutions of the ΔE_1, ΔE_2 and E detectors increased by a factor of two.

5. Summary

The detector telescopes for the planned measurement of double-differential emission cross sections for light ions at the n_TOF facility will consist of ion-implanted silicon diodes of various thicknesses used as transmission detector and plastic scintillators and, eventually, $CeBr_3$ detectors as stop detectors. Different ion species will be discriminated using the ΔE-E method. The resolution of the diodes using different analog pulse processing modules was studied in experiments with protons and alpha particles from radioactive sources and scattered ion beams. The results show that particle identification should also work at energies where the range of the ions is only slightly larger than the thickness of the thinnest ΔE detector in the telescopes.

The intense γ-flash at the n-TOF facility will provide a challenge for the dynamic range of the detector and eventually cause saturation effects. Monte Carlo simulations showed that the charge pulse induced by the γ-flash could reduce the dynamic range of the preamplifier available for registering valid neutron-induced events. Therefore, gating circuits between detector and preamplifier were tested to suppress the γ-flash signal. For the latest version of these modules, almost no additional deterioration of the detector resolution by the gating circuit was found.

Despite these preparatory tests, final conclusions about the performance of the telescopes will only be possible after the first test run at n_TOF which is scheduled for May 2022.

References

[1] J. Farah et al. Med. Phys. **42** (2015) 2572-2584
[2] D. Satoh et al., Nucl. Instr. and Meth. in Phys. Res. A **644** (2011) 59-67
[3] X. G. Xu et al., Phys. Med. Biol. **53** (2008) R191-R241
[4] U. Schneider, R. Hälg, Front. Oncol. **5** (2015) 235
[5] N. Olsson et al., Nucl. Phys. A **559** (1993) 368-400
[6] U. Tippawan et al. Phys. Rev. C **79** (2009) 064611
[7] S. Hirayama et al., Progr. Nucl. Sci. and Techn. **1** (2011) 69
[8] U. Tippawan et al., Phys. Rev. C **73** (2006) 034611
[9] Y. Watanabe et al., Progr. Nucl. Sci. and Techn. **4** (2014) 569-573
[10] J.-C. David, Eur. Phys. J. A **51** (2015) 68
[11] International Commission on Radiation Units and Measurements, *Nuclear Data for Neutron and Proton Radiotherapy and for Radiation Protection*, ICRU Report **63**, Bethesda, Maryland, USA (2000)
[12] L. Audouin et al., Proposal INTC-P-507 to the ISOLDE and Neutron Time-of-Flight Committee, May 2017
[13] C. Guerrero et al., Eur. Phys. J. A **49** (2013) 27
[14] P.G. Young, E.D. Arthur, M.B. Chadwick, *Comprehensive Nuclear Model Calculations: Introduction to the Theory of the GNASH Code*, Los Alamos National Laboratory Document LA-2343-MS (1992)
[15] S. Urlass et al., Nucl. Instr. and Meth. in Phys. Res. A **1002** (2021) 165297